Mechanical Properties of Materially and Geometrically Gradient Cellular Structures Manufactured with SLS 3D Printer Applicable as a Bone Implant

Ali Salehi, Alireza Daneshmehr*, Kiyarash Aminfar
School of Mechanical Engineering,
University of Tehran, Tehran, Iran
E-mail: ali.salehi1993@ut.ac.ir, daneshmehr@ut.ac.ir, kaminfar@ut.ac.ir
*Corresponding author

Received: 10 May 2021, Revised: 6 July 2021, Accepted: 10 July 2021

Abstract: Cellular structures are broadly used because of their exclusive properties in tissue engineering. This research proposes a new method, both in design and manufacturing, to engineer their mechanical properties considering gradient material and geometrical features and evaluate the possibility of using created structures as bone implants. Schwarz-primitive surface has been utilized to design cellular structures with different porosities and unit cell sizes. A total of 18 cellular structures were designed and fabricated using the SLS 3D printer with a new unconventional approach in adjusting the settings of the machine, and their mechanical properties were extracted. The structures' internal properties were evaluated using the FESEM. Comparing the mechanical compressive test results showed that adjustments in material and geometry improved mechanical properties (such as the compressive moduli, compressive strength, and yield strength). For instance, in 3 mm samples, the elastic modulus in material gradient and geometrical gradient structures is 20% and 73 % higher than the minimum values of the uniform structure. FESEM imaging revealed that adjusting the absorbed energy by powders (controlled by laser characteristics) leads to the formation of natural voids with diameters in the range of 6 to 144 μm for the gradient structures. Evaluation of the designed structures showed that 6 of them (4 uniform porosity and 2 geometrically gradient) have mechanical behavior of the desired tissue. The research outcomes can assist in optimizing manufactured parts by SLS 3D printers with internal and external controlled properties to obtain more desirable mechanical characteristics, especially for tissue engineering applications.

Keywords: Additive Manufacturing, Cellular Structures, Gradient Structures, Selective Laser Sintering, Tissue Engineering, Triply Periodic Minimal Surface

How to cite this paper: Ali Salehi, Alireza Daneshmehr, and Kiyarash Aminfar, "Mechanical Properties of Materially and Geometrically Gradient Cellular Structures Manufactured with SLS 3D Printer Applicable as a Bone Implant", Int J of Advanced Design and Manufacturing Technology, Vol. 15/No. 1, 2022, pp. 143–155.
DOI: 10.30495/admt.2022.1930119.1283.

Biographical notes: Ali Salehi is a graduate MSc student from the School of Mechanical Engineering, University of Tehran, Iran, in 2019. His research interests include Additive Manufacturing, Smart and Lightweight Structures, Bone Tissue Engineering, and Bio-inspired Soft Robotics. **Alireza Daneshmehr** is an Associate Professor at the School of Mechanical Engineering, University of Tehran, Iran. He received his PhD in Mechanical Engineering from Amirkabir University of Technology in 2006. His research interests include Additive Manufacturing, Composite Structures and Tissue Engineering. **Kiyarash Aminfar** received his MSc in Mechanical Engineering from University of Tehran, Iran in 2018. His research interests include Advanced Manufacturing, Structural Health Monitoring and Data Analysis.

1 INTRODUCTION

Design, fabrication, and mechanical analysis of cellular structures are currently widely studied by many researchers due to their low density, controllable internal material properties, and high surface-to-volume ratio [1-4]. The applications of these remarkable structures cover different industries, such as automotive and aerospace. However, it is not limited to this, and they are utilized as tissue scaffolds to heal bone defects, heat exchangers with optimized design, and filters [5-7].

The Triply Periodic Minimal Surface (TPMS) is one of the theories that can be exploited to design controlled and optimized structures with different unit cells and porosities [8]. In recent years, studying and optimizing cellular structures' mechanical properties using TPMS have been an exciting subject for many researchers [7], [9-11]. TPMS could be applied to design cellular structures with gradient properties either by changing geometrical or material parameters. Gradient cellular structures are suitable for bone implant design cases, considering the desired bone tissue behavior. By optimizing the structure's mechanical attributes, a customized implant can be produced for a particular patient's bone (such as hip bone or jaw). In that case, the structure's mechanical properties would reflect the tissue's properties correctly [12-15]. Another example is the topology optimization of a bending beam applicable in the aerospace and automotive industries [16]. Additive Manufacturing (AM), a state-of-the-art technology, can be used to make customized and controlled cellular structures.

One of the AM methods is Selective Laser Sintering (SLS), which is capable of customizing both internal and external properties of cellular structures [17-19]. SLS employs powdered materials to perform selectively sintering operations layer by layer to produce a complex 3D object [20]. The fabricated part using SLS shows suitable mechanical properties, which can be used as end-use production [21]. Some parameters have to be optimized to produce a desirable cellular structure in SLS 3D printing.

These parameters are laser Power (P), Laser beam Speed (LS), and Hatch Space (HS). The relation between these parameters can determine the energy absorbed in powders called Energy Density (ED), as given in Equation (1). Energy density is a criterion to determine the density of parts in SLS 3D printing [20]. For instance, by increasing the laser power in SLS 3D printing, ED is increased, and as a result, a denser part with fewer holes is created. Thus, by adjusting the ED, the volume fraction (porosity) of cellular structures can be adjusted [22-23].

$$ED = P/(HS \times LS) \tag{1}$$

This research aims to investigate and compare the mechanical properties of cellular structures designed based on the Schwarz-primitive minimal surface, considering the material and geometrical gradient properties. Some unique initial settings of the SLS printer are adjusted through the manufacturing process. A total of 18 cellular structures with three different unit cell sizes from 3 to 5 millimeters and different porosities in the range of 40% to 70% are fabricated using the selective laser sintering 3D method. The mechanical properties of the structure, such as elastic modulus and yield stress, are measured by mechanical compressive tests. Field emission scanning microscopy is utilized to obtain the internal characteristics of the material gradient cellular structures. Finally, as a practical example, the application of proposed cellular structures as a bone implant for cancellous bones is presented. The results are evaluated and discussed, which can help both researchers and manufacturers, especially in the field of tissue engineering, to obtain their optimized fabricated parts by SLS 3D printers with internal and external controlled properties.

2 METHODOLOGY

2.1. Design Procedure

The theory of Triply Periodic Minimal Surface (TPMS) is used for cellular structures' design. TPMS can be introduced by an implicit function (f (x,y,z)) in Equation (2), where t specifies the deviation from the base levels of the shape and determines the volume fraction of the minimal surfaces [24-25].

$$f(x,y,z) = t \qquad -1 \le t \le 1 \tag{2}$$

Among the minimal surfaces, there are Schwarz-primitive, Schwarz-diamond, and Schoen-gyroid [26-28]. Figure 1 shows a unit cell of these three surfaces. The Schwarz-primitive minimal surface's fluid permeability is higher than other minimal surfaces, which is a good factor for many applications, especially tissue scaffolds and bone implants [24].

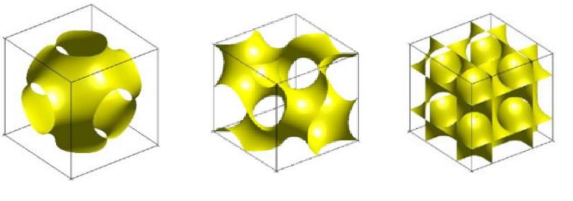

(a) **(b)** **(c)**

Fig. 1 Three examples of minimal surfaces: (a): Schwarz-primitive surface, (b): Schoen-gyroid surface, and (c): Schwarz-diamond surface [29].

Considering the advantages of the Schwarz-primitive surface in tissue engineering, it was exploited in this study to prepare cellular structure shapes. Equation (3) describes the Schwarz-primitive minimal surface function, f_p, where n_i is the number of the repeated unit cells in i-direction, and L_i is the size of each unit cell in mm [25].

$$f_P(x,y,z) = \cos(\lambda_x x) + \cos(\lambda_y y) + \cos(\lambda_z z) \quad (3)$$

$$i = x,y,z \qquad \lambda_i = 2\pi \times n_i / L_i$$

Figure 2 shows a simple unit cell used in this study. Here, three sets of mechanical and geometrical attributes of the Schwarz-primitive unit cell are considered, as demonstrated in "Fig. 3".

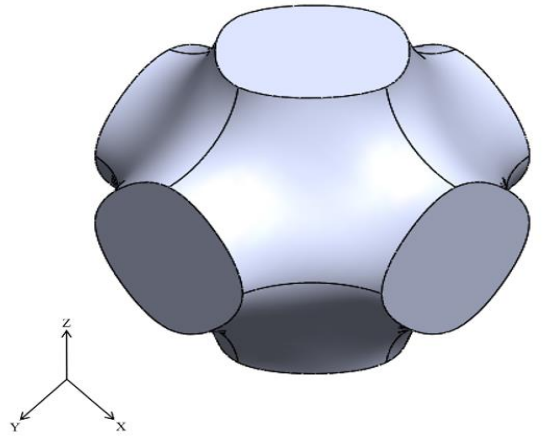

Fig. 2 The Schwarz-primitive unit cell used in this study.

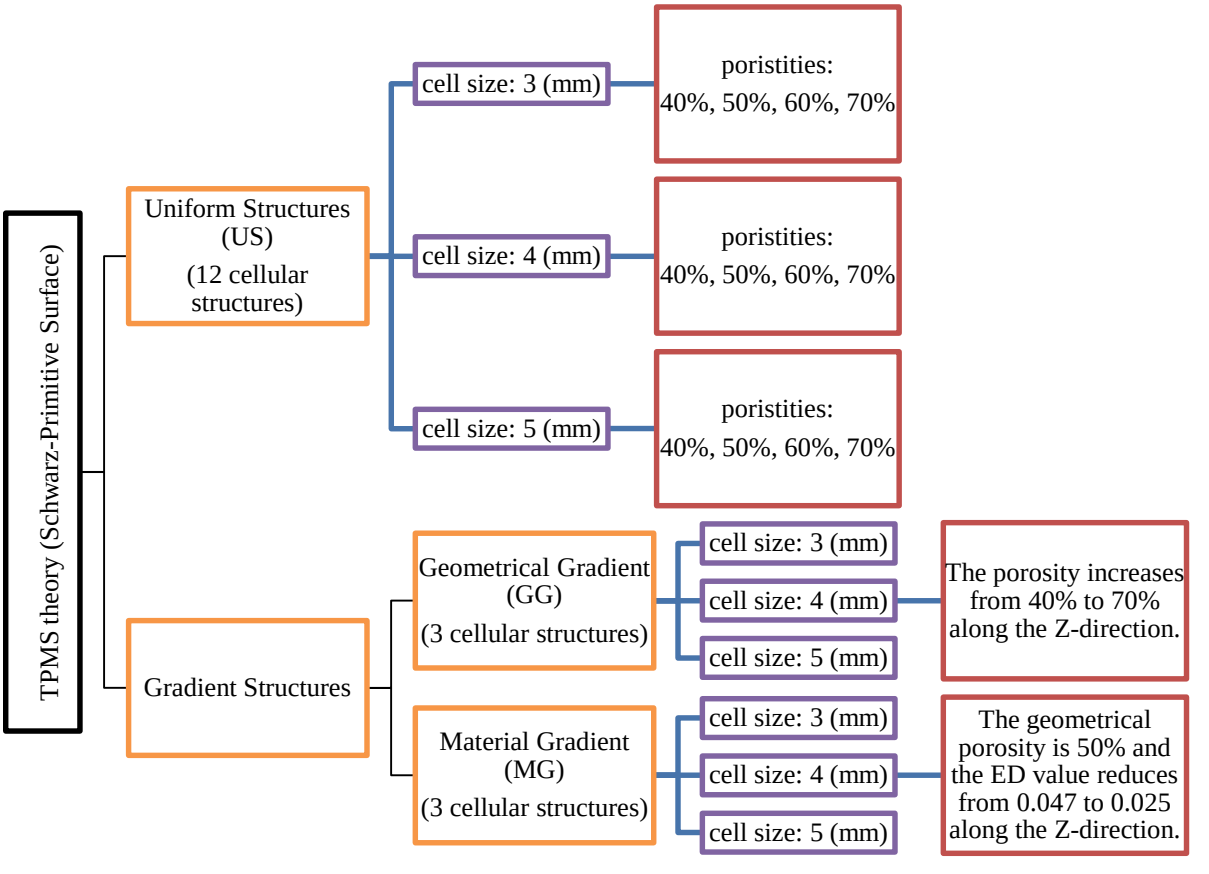

Fig. 3 Schematic of the design procedure.

First, 12 Uniform Structures (US) with uniform porosity along the Z-axis were designed and manufactured with the following attributes: 3 different unit cell sizes (3, 4, and 5 (mm)) and four different porosity values (40,50,60 and 70%). Note that in this research, the size of 3 and 4 (mm) parts was 24*12*12 (mm^3), and the dimensions of the 5 (mm) parts were 30*15*15 (mm^3). In the next steps, three cellular structures with gradient porosity by changing the unit cells' porosity along the Z-axis were produced, which are called Geometrical Gradient (GG)

structures. The unit cell sizes were 3, 4, and 5 (mm), and the porosity value of unit cells varied from 40% to 70%. Finally, three cellular structures with gradient material porosity along the Z-axis were created by changing the SLS machine's laser power from 10 to 19 (watts), as is discussed in the literature [29]. These parts are called Material Gradient (MG) structures. The manufactured parts had 3, 4, and 5 (mm) unit cell sizes, and all of the MG structures had a geometry porosity of 50%. Figure 4 illustrates the material porosity of the structures along the Z direction. According to Equation (1), the ED of the structures was calculated and was in the range of 0.025 (J/mm^2) to 0.0475 (J/mm^2) along the Z-axis.

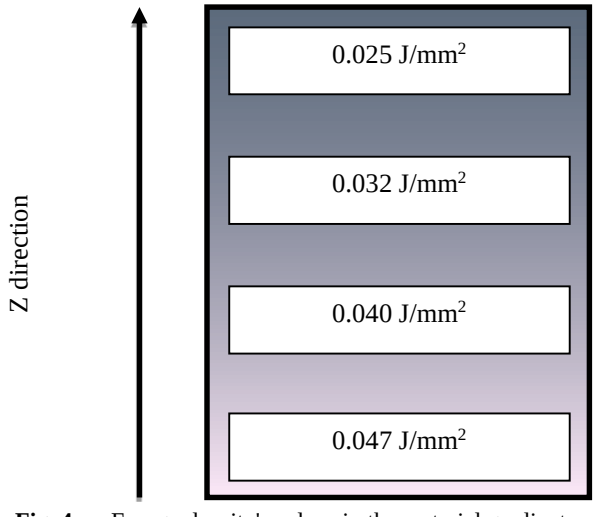

Fig. 4 Energy density's values in the material gradient structures.

2.2. Modelling Cellular Structures

A code was developed in MATLAB, employing Schwarz-primitive minimal surfaces (Equation (3)) to draw and create cellular shapes. According to Equation (3), by changing the parameter t, the volume fraction and porosity of the cell structure can be adjusted. After creating the initial geometry in MATLAB, a function was used to transform the geometry into a Standard Triangle Language (STL) file. Then, the Geomagic plug-in for SOLIDWORKS was utilized to obtain desired cellular structures with smooth surfaces. The output of the design steps in this research can be seen in "Fig. 5".

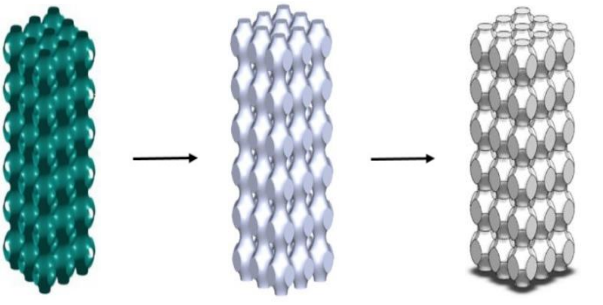

Fig. 5 Design steps: (a): 3D model extracted from the MATLAB script, (b): Converted STL file to Step file, and (c): Smoothed surfaces of the model.

2.3. Manufacturing of the Cellular Structures

All cellular structures were manufactured by the T1 R230 Pro SLS 3D printer. Polyamide 12 (the commercial name is PA2200), a commonly used biocompatible material for SLS 3D printer, was used as the raw material. The powder had a density of 1.01 (g/cm^3), and its mechanical properties under various printer settings (different EDs) were tested according to ASTM-D695 [30] for four models having 24*12*12 (mm^3) sizes. These structures are called solid bulks.

In "Table 1", the manufacturing parameters for structures are written concerning different structure types. The parameters for the uniform and geometrical gradient structures are the same. Each material gradient structure was divided into four sections, having various EDs coming from different laser powers.

Table 1 Manufacturing Parameters utilized in SLS 3D printer for fabricating cellular structures.

Structure Type	Section	P (W)	LS (mm/s)	HS (mm)	Layer Thickness (mm)	ED (J/mm2)
Uniform Structures (US)	-	16	1600	0.250	0.120	0.040
Geometrical Gradient (GG)	-	16	1600	0.250	0.120	0.040
Material Gradient (MG)	1	10	1600	0.250	0.120	0.025
	2	13	1600	0.250	0.120	0.0325
	3	16	1600	0.250	0.120	0.040
	4	19	1600	0.250	0.120	0.0475

The porosity of the manufactured structure can be represented by Equation (4) [31], in which, V_m is the total volume of cellular structures, V_p is the actual volume of material, W_m is the mass of the cellular structures, and ρ is the density of the material.

$$P(\%) = \frac{V_m - V_p}{V_m} * 100 = \frac{V_m - \left(\frac{W_m}{\rho}\right)}{V_m} * 100 \quad (4)$$

The Adam scale (model HCB 1002) with a 0.01g resolution is used to determine the mass of all 18 cellular structures and four solid bulks to calculate structures' porosity. In "Fig. 6", some manufactured cellular structures can be seen concerning different unit cell sizes (left to right: 3, 4, and 5 (mm)). Figure 6a represents examples of uniform cellular structures with 50% porosity, and "Figs. 6b and 6c" represent GG structures and MG structures, respectively.

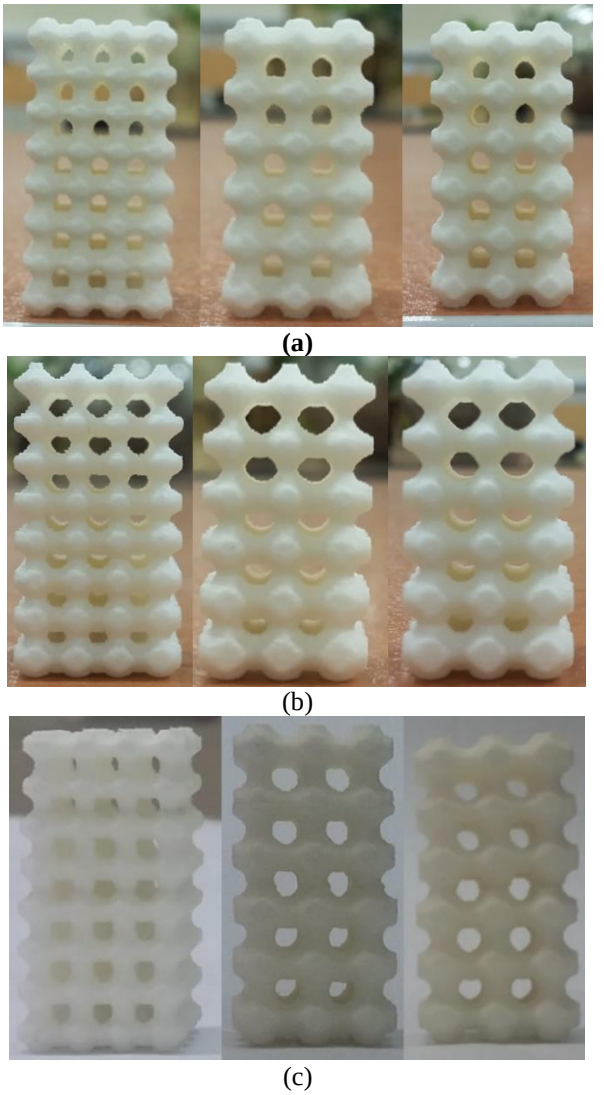

(a)

(b)

(c)

Fig. 6 Some manufactured cellular structures: (a): uniform structures with 50% porosity, (b): geometrical gradient structures, and (c): material gradient structures.

2.4. Mechanical Testing

The mechanical compression tests were conducted on all structures by an Instron-4208 testing machine at a strain rate of 1 (mm/min), according to ASTM D695 [30], as shown in "Fig.7". The elastic modulus and the yield stress considering 0.2% strain offset for each structure were obtained using the stress-strain curve.

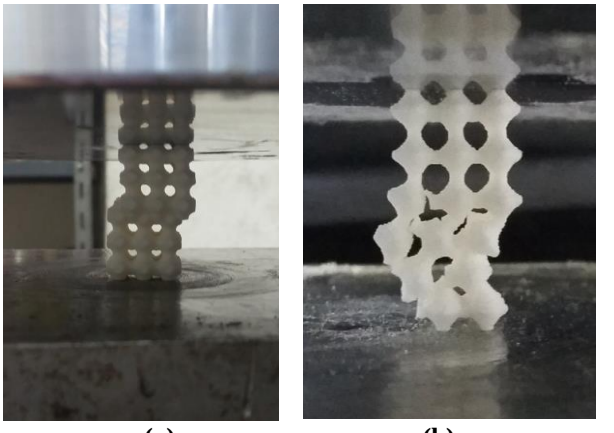

(a) **(b)**

Fig. 7 Mechanical testing on cellular structures: (a): material gradient structure, and (b): uniform cellular structures with 60% porosity and 4 (mm) unit cell size.

2.5. Morphological and Internal Characteristics of Cellular Structures

The structures were imaged using Field Emission Scanning Electron Microscope (FESEM) HIT 4160 02, under vacuum conditions with pressure of 1e-7 (Torr), approximately 1.33322e-5 (Pa), to observe the differences in the gradient properties of MG structures ("Fig. 8a"). Before scanning, a 1.5 (nm) gold layer was coated on the structures to enhance the imaging process ("Fig. 8b").

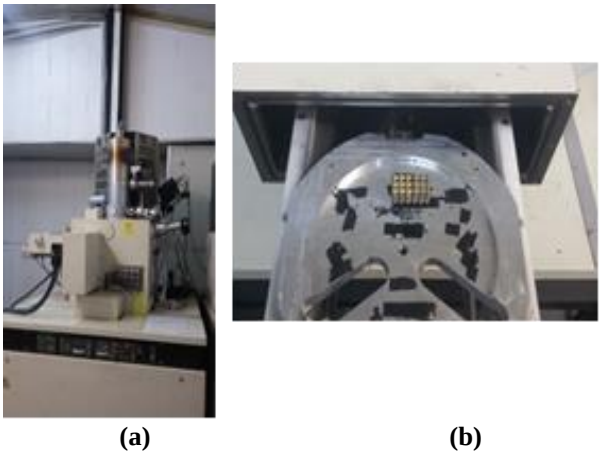

(a) **(b)**

Fig. 8 Morphological tests setup: (a): FESEM, and (b) a sample of cellular structures coated with a gold layer.

3 RESULTS AND DISCUSSION

3.1. Manufacturing Characteristics of Cellular Structures

The utilized energy density in the manufacturing process directly influences material porosity, and structures with gradient properties could be created by adjusting this parameter. After fabricating structures, their actual

density and amount of porosity were measured. Figure 9 shows the effect of energy density on actual density and the amount of porosity for four solid bulks. By increasing the ED from 0.025 to 0.047 (J/mm^2), the density of solid bulks changed from 0.905 to 0.963 (g/cm^3). Thus, the ratio of porosity in solid bulk models varied from 10.36 to 4.61, which means that a better powder fusion or, in other words manufacturing a denser structure has happened in solid models by increasing the ED. Table 2 shows the deviation between actual and designed porosity for uniform and gradient cellular structures. Different produced structures have been named according to their unit cell dimensions and porosities (i.e., US-3mm40% refers to a uniform structure part with 3 (mm) unit cell size and 40% porosity). Further evaluation in the results of Table 2 reveals that in all cellular structures with a uniform porosity, by increasing the value of intended porosity, the deviation between actual and designed porosity at first ascends then after 60% porosity declines.

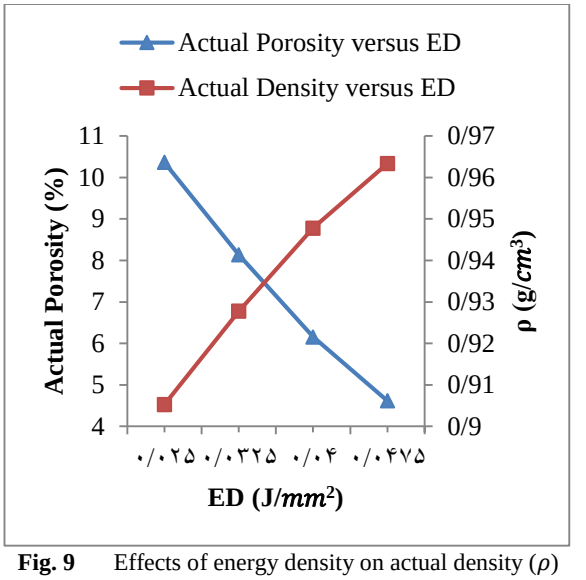

Fig. 9 Effects of energy density on actual density (ρ) and amount of porosity for four solid bulks.

Table 2 The absolute deviation between actual porosity and design porosity for uniform and gradient cellular structures

Type of Structure	Model Name	Design Porosity (%)	Actual porosity (%)	Absolute Deviation (%)
Uniform Structures	US-3mm40%	40	42.13	2.13
	US-3mm50%	50	52.6	2.6
	US-3mm60%	60	66.15	6.15
	US-3mm70%	70	72.69	5.69
	US-4mm40%	40	42.13	2.13
	US-4mm50%	50	52.31	2.31
	US-4mm60%	60	64.41	4.41
	US-4mm70%	70	73.67	3.67
	US-5mm40%	40	40.3	0.3
	US-5mm50%	50	51.13	1.13
	US-5mm60%	60	63.41	3.41
	US-5mm70%	70	71.85	1.85
Geometrical Gradient	GG-3mm	55 (Mean)	50.52	-4.48
	GG-4mm	55 (Mean)	52.55	-2.45
	GG-5mm	55 (Mean)	53.19	-1.81
Material Gradient	MG-3mm	55 (Mean)	57.18	2.18
	MG-4mm	55 (Mean)	54.28	-0.72
	MG-5mm	55 (Mean)	54.37	-0.63

In GG structures, the actual average porosity for models is less than the average calculated design porosity, which might be caused by the manufacturing parameters of the SLS 3D printer, such as gradient temperature in the powder bed, which adversely affected the density of structures, and consequently, changed the porosity of cellular structures. In all types of structures, it is observed that structures with bigger unit cell sizes have smaller deviations between their intended and actual porosities, which shows that for models with smaller cavities, the design and fabrication are more similar. In MG structures, the calculated porosity and test outcomes are in good agreement. The overall analysis of deviations in design and tests depicts that MG structures are more akin to the intended shapes compared to GG structures. Hence, the changes in the geometry of structures are more effective than changes in material properties in terms of the SLS 3D printer's manufacturing accuracy.

3.2. Mechanical Tests Results

3.2.1. Mechanical Properties of the Material with Different Energy Densities

The stress-strain diagram for solid bulks is presented in "Fig. 10". The elastic modulus of materials declines by increasing the ED, but the yield stress, strain at yield point, and ultimate compression strength amplify. As mentioned in [32], when ED reaches the top value, the powder particles are damaged or burnt by excess heat from the laser.

So it is expected that this effect causes the elastic modulus to decrease even in small quantities. However, the range of elasticity and also yield stress is increased. Thus, using SLS 3D printing as a manufacturing method can improve the elastic range of structures, which is an essential feature for many applications. The mechanical characteristic of four solid bulks is illustrated in "Table 3".

Table 3 Mechanical properties of solid bulks

Part Number	ED (J/mm^2)	E (GPa)	σ_y (MPa)	σ_{UC} (MPa)	ε_y %
1	0.025	1.27	26.28	55	2.15
2	0.0325	1.23	30.64	61	2.8
3	0.04	1.17	41	71	4.2
4	0.0475	1.16	44.5	78	4.7

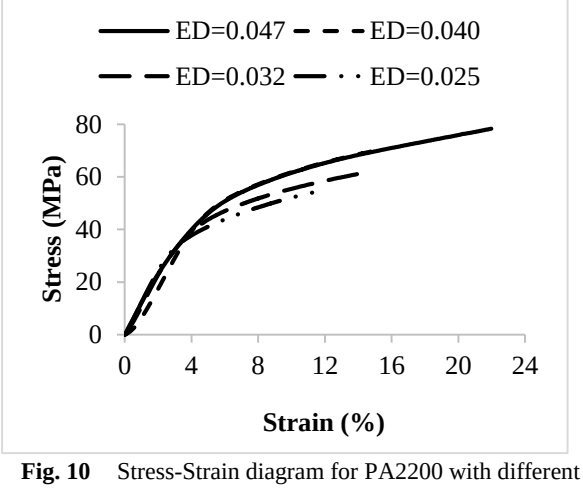

Fig. 10 Stress-Strain diagram for PA2200 with different ED values.

3.2.2. Mechanical Properties of Cellular Structures

The outcome of extracting structures' mechanical properties is presented in this section. Figure 11 shows the stress-strain diagram for all cellular structures with different porosities. "Table 4" summarizes all the attributes obtained from "Fig. 11", including the elastic modulus, compressive strength, yield strength, and yield strain. It should be noted that for the uniform structures, these attributes are both in the range of actual tissue (for different porosities) and the average values. However, in GG and MG structures, only average quantities exist because the porosity is not identical.

As presented in "Table 4" and illustrated in "Fig. 12", by increasing the porosity from 40 % to 70 %, elastic modulus decreases in uniform cellular structures. The elastic modulus for both geometrical and material gradient structures is less than the average elastic modulus of uniform structures. For instance, in 3 (mm) cellular structures, the uniform structure's average elastic modulus is 0.32 (GPa). In comparison, for geometrical and material gradient structures, this value is 0.26 and 0.13 (GPa), respectively. However, suppose the elastic modulus of gradient cellular structures is compared with the elastic modulus range in uniform cellular structures.

In that case, it will be found that the elastic modulus in gradient structures has been improved in comparison to uniform structures. For example, in GG-3mm and MG-3mm, the elastic modulus is 73 % and 20 % more than the minimum value of elastic modulus in the uniform structure, respectively. This result confirms that gradient properties in cellular structures can improve the overall elastic behavior of the structure.

Figure 13 explains the effect of porosity on the compressive strength of cellular structures. According to this figure and "Table 4", the compressive strength of cellular structures with geometrical and material gradient properties is higher than the minimum value of the aforementioned parameter in uniform cellular structures. For instance, in structures with 3 (mm) cell size, the difference between US and GG structures and US and MG structures is 1200% and 800%, respectively. Besides, the results show that the compressive strength in MG structures is more than GG structures, which indicates that modifications in the parameters of the SLS 3D printer, such as laser power, have a more significant impact on the compressive strength improvement.

Table 4 Mechanical properties of cellular structures

Type of Structures	Model Name	Elastic Modulus (GPa)	Compressive Strength (MPa)	Yield Strength (MPa)	Yield Strain (%)
Uniform Structures	US-3mm40%	0.43	30	16	3.5
	US-3mm50%	0.38	21.3	11.5	3.1
	US-3mm60%	32	4.8	1.17	0.74
	US-3mm70%	0.16	1.4	0.5	0.65
	US-4mm40%	0.45	37	13.7	3.4
	US-4mm50%	0.35	20.5	9.3	2.9
	US-4mm60%	0.235	9	2.1	1.2
	US-4mm70%	0.18	1.8	0.8	0.55
	US-5mm40%	0.52	25.3	14.2	2.9
	US-5mm50%	0.38	21	10	2.8
	US-5mm60%	0.28	9	2.2	1
	US-5mm70%	0.16	2.1	0.6	0.55
Geometrical Gradient	GG-3mm	0.26	18	7.2	3.6
	GG-4mm	0.32	6	5.7	5.5
	GG-5mm	0.21	9	3.8	2
Material Gradient	MG-3mm	0.13	12	8	6.6
	MG-4mm	0.2	16	6.4	3.4
	MG-5mm	0.22	15	6.5	3.15

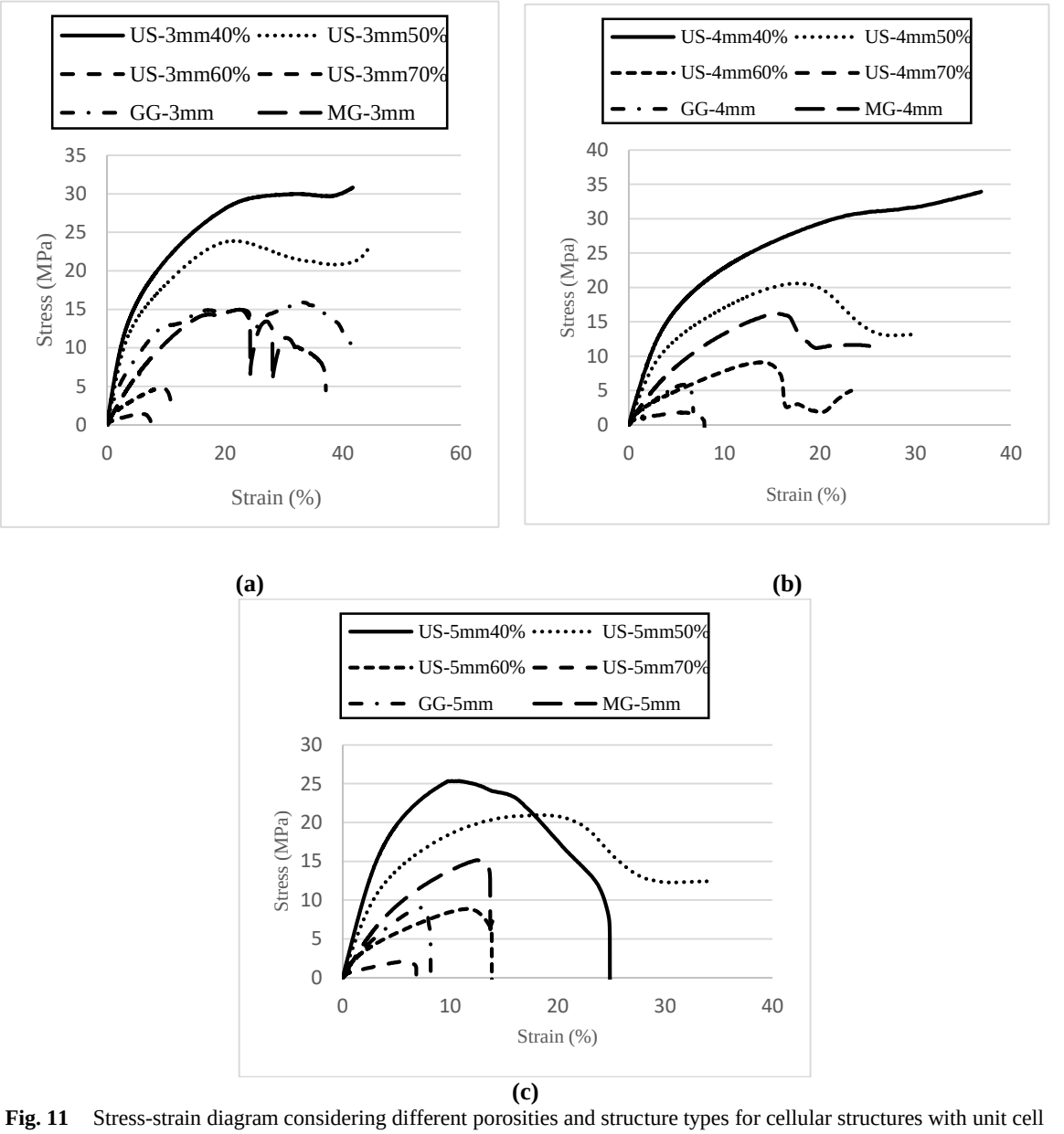

Fig. 11 Stress-strain diagram considering different porosities and structure types for cellular structures with unit cell sizes of: (a): 3 (mm), (b): 4 (mm), and (c): 5 (mm).

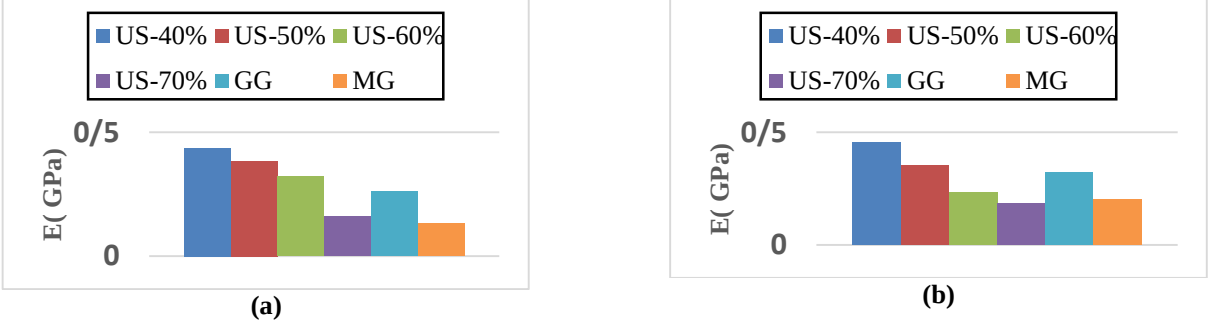

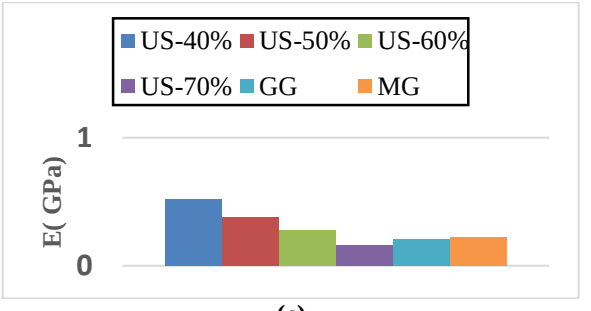

(c)

Fig. 12 Elastic modulus of cellular structures considering different porosities and structure types in: (a): 3 (mm), (b): 4 (mm), and (c): 5 (mm) structures.

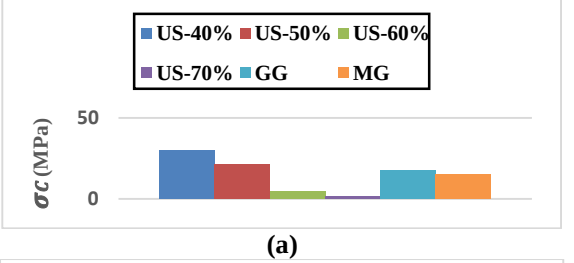

(a)

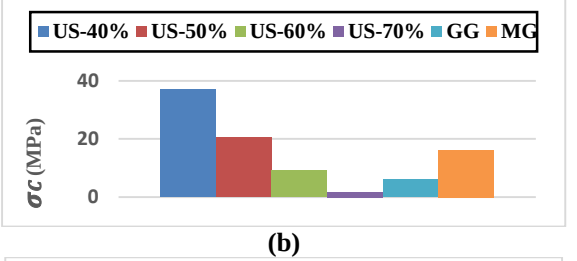

(b)

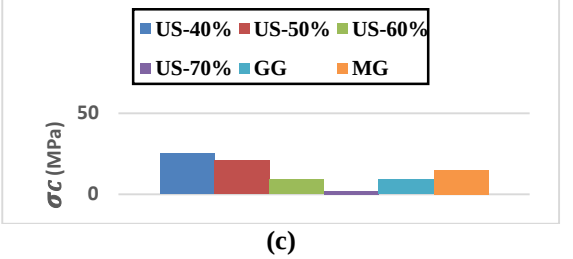

(c)

Fig. 13 Compressive strength of cellular structures considering different porosities and structure types in: (a): 3 (mm), (b): 4 (mm), and (c): 5 (mm) structures.

As shown in "Fig. 14", the gradient properties have a notable impact on cellular structures' yield strength. For instance, in MG cellular structures, yield strength is increased compared to the average yield strength of uniform cellular structures (except in MG-5mm with a difference of 3%). On the other hand, in GG cellular structures, yield strength values are lower than the average values in uniform structures (the differences are between 0.2% and 43%). However, there is a substantial increase in this value compared to the minimum yield strength of the uniform cellular structures, which displays improvement in the structure's mechanical properties ("Table 4").

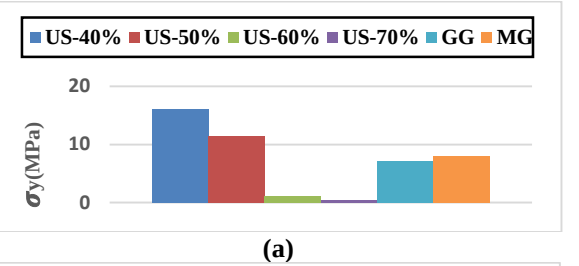

(a)

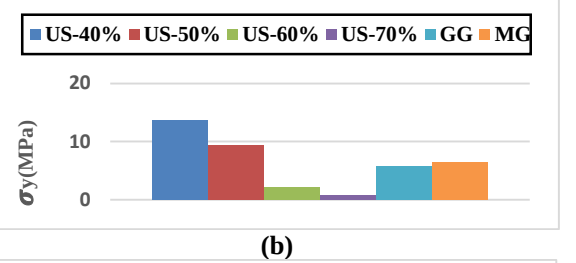

(b)

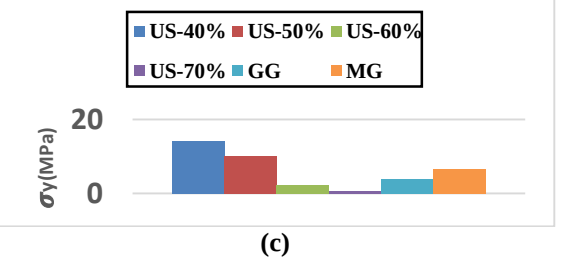

(c)

Fig. 14 Yield strength of cellular structures considering different porosities and structure types in: (a): 3 (mm), (b): 4 (mm), and (c): 5 (mm) structures.

Figure 15 shows the strain at the yield point of the cellular structures. For all gradient cellular structures, the yield strains are higher than the average yield strain in uniform cellular structures. The most significant difference is observed in MG cellular structures with 3 (mm) unit cell size, which is three times bigger than the average yield strain in the corresponding uniform cellular structure. Thus, it can be seen that the gradient properties (whether material or geometrical) seriously affect the strain value at the yield point and lead to higher yield strains in comparison to uniform cellular structures.

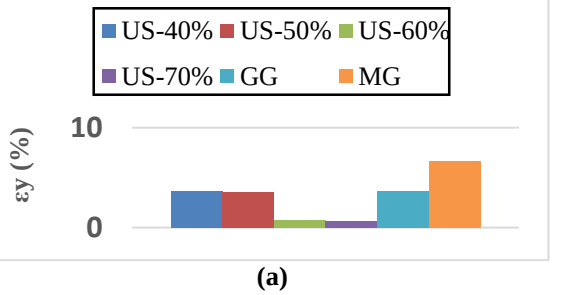

(a)

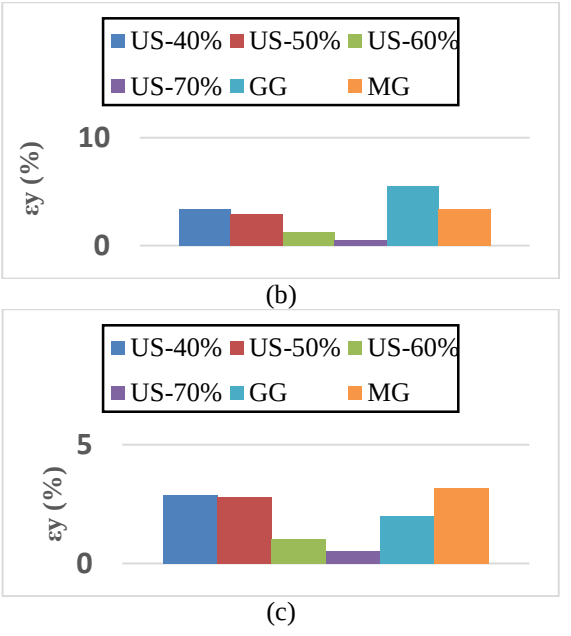

Fig. 15 Yield strain of cellular structures considering different porosities and structure types in: (a): 3 (mm), (b): 4 (mm), and (c): 5 (mm) structures.

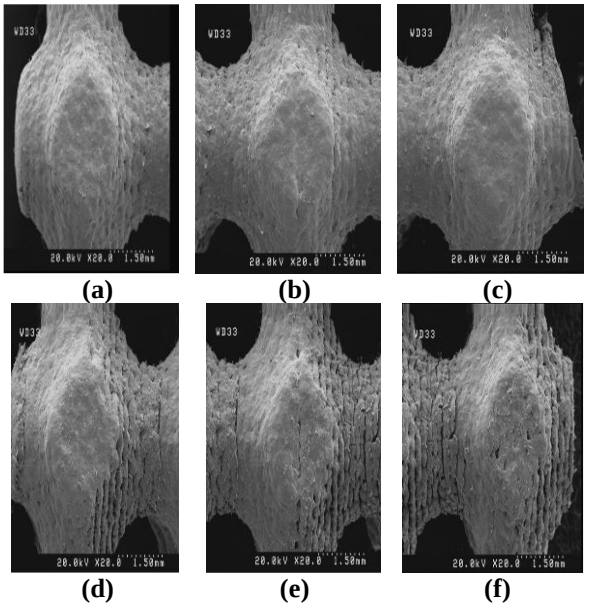

Fig. 16 The influence of increasing the porosity value by decreasing ED along the Z-axis: (a): z=5 (mm), (b): z=10 (mm), (c): z=15 (mm), (d): z=20 (mm), (e): z=25 (mm), (f): z=30 (mm).

3.3. Morphological and Structural Properties of Material Gradient Structures

The structural properties of MG cellular structures were analyzed using the FESEM imaging method. MG-3mm and MG-4mm structures' dimensions were 24*12*12 (mm^3), but MG-5mm structures' length, width, and height were 15, 15, and 30 (mm), respectively. Here the results are given for different sections of the MG-5mm part in "Fig. 16 and Fig. 17". As shown in "Fig.16", by decreasing the ED along the Z-axis, the size of voids in the cellular structure increased, and consequently, the porosity amplified along the Z-axis. Figure 17 illustrates the size of the created voids, which varies from 6 to 144 microns. This examination shows the influence of modifications in the ED, which is the base step of fabricating intended MG properties in cellular structures.

3.4. Case Study: Application of Proposed Cellular Structures as an Implant for Trabecular Bone

One of the applications of cellular structures is their use as implants for bone tissue. As an applicable case study, the use of fabricated cellular structures as a cancellous bone implant is investigated. The cancellous bone has a porosity between 30 and 90 % [33], and its elastic modulus is in the range of 50 and 500 MPa [34]. Also, the compressive strength of this tissue is between 2 and 12 MPa [34].

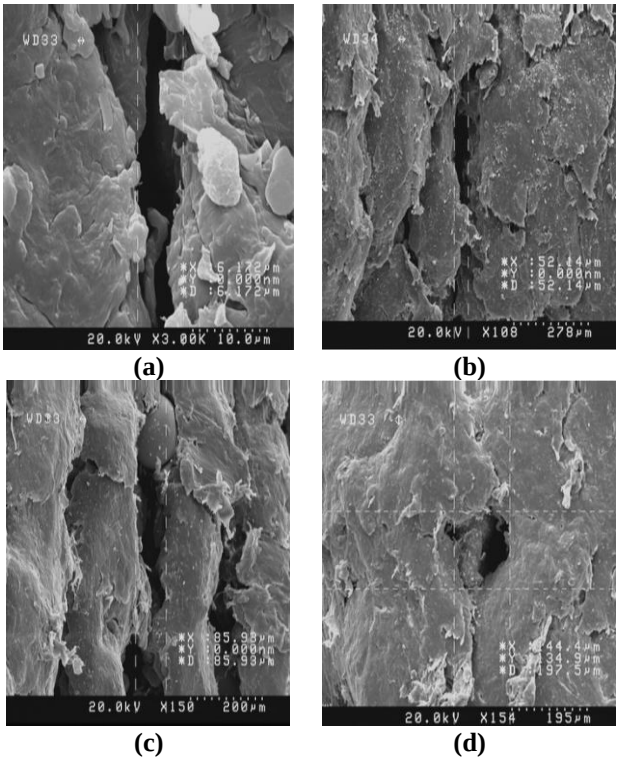

Fig. 17 The size of created voids in MG structures along the Z-axis: (a) z=7.5 (mm); (b) z=15 (mm); (c) z=22.5 (mm); (d) z=30 (mm).

According to Table 4, the comparison between fabricated parts and mentioned bone showed that except for the uniform structure with a unit cell size of 5 (mm) and a porosity of 40%, all other printed structures have an elastic modulus in the range of the porous bone tissue. Moreover, six of the structures have compressive strength in the range of cancellous bone tissue, including four structures with a uniform porosity (US-3mm60%, US-4mm-60%, US-5mm60%, and US-5mm70%) and two structures with geometrical gradient porosity (GG-4mm and GG-5mm). The compressive strength of fabricated material gradient structures is greater than the compressive strength of cancellous bone tissue and, therefore, will not have similar behavior.

4 CONCLUSION

Cellular structures are used for different purposes, including tissue scaffolds, heat exchangers, and filters, thanks to having unique properties. In the present study, several cellular structures have been designed and manufactured considering various attributes, including materially and geometrically engineered gradient properties. Three types of cellular structures (uniform, geometrical gradient porosity, and material gradient porosity) were fabricated using the Selective Laser Sintering (SLS) 3D printer utilizing minimal Schwarz-primitive surfaces with porosities between 40 and 70 percent. The initial settings of the SLS printer are controlled in an unconventional approach. Also, a case study of utilizing cellular structures as a bone implant was performed. The structures with gradient properties prove to have better mechanical properties compared to uniform cellular structures, especially on yield strength and strain at the yield point. Moreover, it is observed that the material gradient structures have better mechanical characteristics, such as yield stress, in comparison to geometrical gradient ones. The designed cellular structures were examined in terms of mechanical and structural properties to be used as cancellous bone tissue, and six structures comply with the mechanical and structural characteristics of the desired texture and are suitable for this application. In this research, a new procedure for adjusting manufacturing parameters in the SLS process regarding the porosity of structures has been presented, which can be exploited to obtain optimized and desired cellular structures with controlled internal and external properties.

REFERENCES

[1] Maconachie, T., Leary, M., Lozanovski, B., Zhang, X., Qian, M., and Faruque, O., et al. SLM Lattice Structures: Properties, Performance, Applications and Challenges, Mater Des, Vol. 183, 2019, pp. 108137, DOI:10.1016/j.matdes.2019.108137.

[2] Alketan, O., Abu Al-Rub, R., and Rowshan, R., The Effect of Architecture On the Mechanical Properties of Cellular Structures Based On the IWP Minimal Surface, J Mater Res, Vol. 33, 2018, pp. 1–17, DOI:10.1557/jmr.2018.1.

[3] Yoo, D. J., Advanced Porous Scaffold Design Using Multi-Void Triply Periodic Minimal Surface Models with High Surface Area to Volume Ratios, Int J Precis Eng Manuf, Vol. 15, 2014, pp. 1657–66, DOI:10.1007/s12541-014-0516-5.

[4] Liu, Y, Wang, L., Enhanced Stiffness, Strength and Energy Absorption for Co-Continuous Composites with Liquid Filler, Compos Struct, Vol. 128, 2015, pp. 274–83, DOI:10.1016/j.compstruct.2015.03.064.

[5] Qian, T., liu, D., Tian, X., Liu, C., and Wang, H., Microstructure of TA2/TA15 Graded Structural Material by Laser Additive Manufacturing Process, Trans Nonferrous Met Soc China, Vol. 24, 2014, pp. 2729–36, DOI:10.1016/S1003-6326(14)63404-X.

[6] Wadley, H. N. G., Queheillalt, D. T., Thermal Applications of Cellular Lattice Structures. Mater Sci Forum, Vol. 539–543, 2007, pp. 242–7, DOI:10.4028/www.scientific.net/MSF.539-543.242.

[7] Yang, N., Tian, Y., and Zhang, D., Novel Real Function Based Method to Construct Heterogeneous Porous Scaffolds and Additive Manufacturing for Use in Medical Engineering, Med Eng Phys, Vol. 37, 2015, pp. 1037–46, DOI:10.1016/j.medengphy.2015.08.006.

[8] Kapfer, S. C., Hyde, S. T., Mecke, K., Arns, CH., and Schröder Turk, G. E., Minimal Surface Scaffold Designs for Tissue Engineering, Biomaterials, Vol. 32, 2011, pp. 6875–82, DOI:10.1016/j.biomaterials.2011.06.012.

[9] Lu, Y., Zhao, W., Cui, Z., Zhu, H., and Wu, C., The Anisotropic Elastic Behavior of the Widely-Used Triply-Periodic Minimal Surface Based Scaffolds, J Mech Behav Biomed Mater, Vol. 99, 2019, pp. 56–65, DOI:10.1016/j.jmbbm.2019.07.012.

[10] Afshar, M., Anaraki, A. P., Montazerian, H., and Kadkhodapour, J., Additive Manufacturing and Mechanical Characterization of Graded Porosity Scaffolds Designed Based On Triply Periodic Minimal Surface Architectures, J Mech Behav Biomed Mater, Vol. 62, 2016, pp. 481–94, DOI:10.1016/j.jmbbm.2016.05.027.

[11] Li, D., Dai, N., Tang, Y., Dong, G., and Zhao, Y. F., Design and Optimization of Graded Cellular Structures with Triply Periodic Level Surface-Based Topological Shapes, J Mech Des, Vol. 141, 2019, DOI:10.1115/1.4042617.

[12] Wang, S., Zhou, X., Liu, L., Shi, Z., and Hao, Y., On the Design and Properties of Porous Femoral Stems with Adjustable Stiffness Gradient, Med Eng Phys, Vol. 81, 2020, pp. 30–8, DOI:10.1016/j.medengphy.2020.05.003.

[13] Bartolomeu, F., Fonseca, J., Peixinho, N., Alves, N., Gasik, M., and Silva, F. S., et al. Predicting the Output Dimensions, Porosity and Elastic Modulus of Additive Manufactured Biomaterial Structures Targeting Orthopedic Implants, J Mech Behav Biomed Mater, Vol. 99, 2019, pp. 104–17, DOI:10.1016/j.jmbbm.2019.07.023.

[14] Zhao, P., Gu, H., Mi, H., Rao, C., Fu, J., and Turng, L., Fabrication of Scaffolds in Tissue Engineering: A Review, Front Mech Eng, Vol. 13, 2018, pp. 107–19, DOI:10.1007/s11465-018-0496-8.

[15] Dutta, A., Mukherjee, K., Dhara, S., and Gupta, S., Design of Porous Titanium Scaffold for Complete Mandibular Reconstruction: The Influence of Pore Architecture Parameters, Comput Biol Med, Vol. 108, 2019, pp. 31–41, DOI:10.1016/j.compbiomed.2019.03.004.

[16] Sychov, M., Lebedev, L., Dyachenko, S. V., and Nefedova, L. A., Mechanical Properties of Energy-Absorbing Structures with Triply Periodic Minimal Surface Topology, Acta Astronaut, 2017, DOI:10.1016/j.actaastro.2017.12.034.

[17] Chu, C., Graf, G., and Rosen, D., Design for Additive Manufacturing of Cellular Structures. Comput Aided Des Appl, Vol. 5, 2013, pp. 686–96, DOI:10.3722/cadaps.2008.686-696.

[18] Yang, L., Harrysson, O., Cormier, D., West, H., Gong, H., and Stucker, B., Additive Manufacturing of Metal Cellular Structures: Design and Fabrication, JOM, Vol. 67, 2015, DOI:10.1007/s11837-015-1322-y.

[19] Diermann, SH., Lu, M., Zhao, Y., Vandi, L. J., Dargusch, M., and Huang, H., Synthesis, Microstructure, and Mechanical Behaviour of a Unique Porous PHBV Scaffold Manufactured Using Selective Laser Sintering, J Mech Behav Biomed Mater, Vol. 84, 2018, pp. 151–60, DOI:10.1016/j.jmbbm.2018.05.007.

[20] Goodridge, R., Tuck, C., and Hague, R., Laser Sintering of Polyamides and Other Polymers, Prog Mater Sci, Vol. 57, 2012, pp. 229–267, DOI:10.1016/j.pmatsci.2011.04.001.

[21] Mys, N. L., Haverans, T., and Verberckmoes, A. T., Production of Syndiotactic Polystyrene Powder for Part Manufacturing Through SLS, 2014.

[22] Athreya, S., Kalaitzidou, K., and Das, S., Processing and Characterization of a Carbon Black-Filled Electrically Conductive Nylon12 Nanocomposite Produced by Selective Laser Sintering, Mater Sci Eng A-Structural Mater Prop Microstruct Process, Mater Sci Eng A-Struct Mater, Vol. 527, 2010, pp. 2637–42, DOI:10.1016/j.msea.2009.12.028.

[23] Toth Taşcău, M., Raduta, A., Stoia, D., and Locovei, C., Influence of the Energy Density on the Porosity of Polyamide Parts in SLS Process. Solid State Phenom 2012, tific.net/SSP.188.400.

[24] Shin, J., Kim, S., Jeong, D., Lee, H. G, Lee, D., and Lim, J. Y., et al. Finite Element Analysis of Schwarz P Surface Pore Geometries for Tissue-Engineered Scaffolds, Math Probl Eng, 2012, pp. 694194, DOI:10.1155/2012/694194.

[25] Panesar, A., Abdi, M., Hickman, D., and Ashcroft, I., Strategies for Functionally Graded Lattice Structures Derived Using Topology Optimisation for Additive Manufacturing, Addit Manuf, Vol. 19, 2018, pp. 81–94, DOI:10.1016/j.addma.2017.11.008.

[26] Montazerian, H., Davoodi, E., Asadi, M., Kadkhodapour, J., and Solati Hashjin, M., Porous Scaffold Internal Architecture Design Based On Minimal Surfaces: A Compromise Between Permeability and Elastic Properties, Mater Des, Vol. 126, 2017, pp. 98–114, DOI:10.1016/j.matdes.2017.04.009.

[27] Maskery, I., Sturm, L., Aremu, A. O., Panesar, A., Williams, C. B., and Tuck, C. J., et al. Insights into The Mechanical Properties of Several Triply Periodic Minimal Surface Lattice Structures Made by Polymer Additive Manufacturing, Polymer (Guildf), Vol. 152, 2018, pp. 62–71, DOI:10.1016/j.polymer.2017.11.049.

[28] Wang, Y., Periodic Surface Modeling for Computer Aided Nano Design, Comput Des, Vol. 39, 2007, pp. 179–89, DOI:10.1016/j.cad.2006.09.005.

[29] Jande, Y. A. C., Erdal, M., and Dag, S., Production of Graded Porous Polyamide Structures and Polyamide-Epoxy Composites Via Selective Laser Sintering, J Reinf Plast Compos, Vol. 33, 2014, pp. 1017–36. DOI:10.1177/0731684414522536.

[30] Raheem, Z., Designation: D695 − 15 Standard Test Method for Compressive Properties of Rigid Plastics 1, 2019, DOI:10.1520/D0695-15.

[31] Hsieh, W. C., Chang, C. P., Lin, S. M., Morphology and characterization of 3d Micro-Porous Structured Chitosan Scaffolds of Tissue Engineering, Colloids Surf B Biointerfaces, Vol. 57, 2007, pp. 250–5, DOI:10.1016/j.colsurfb.2007.02.004.

[32] Caulfield B, McHugh PE, Lohfeld S. Dependence of mechanical properties of polyamide components on build parameters in the SLS process. J Mater Process Technol 2007;182:477–88. DOI:10.1016/j.jmatprotec.2006.09.007.

[33] Witte, F., Hort, N., Vogt, C., Cohen, S., Kainer, K. U., and Willumeit, R., et al. Degradable Biomaterials Based On Magnesium Corrosion, Curr Opin Solid State Mater Sci, Vol. 12, 2008, pp. 63–72, DOI:10.1016/j.cossms.2009.04.001.

[34] Le Geros, R. Z., Le Geros, J. P., Dense Hydroxyapatite, An Introd. to Bioceram., Vol. 1, World Scientific, 1993, pp. 139–80, DOI:10.1142/9789814317351_0009.